

# CFVNet: An End-to-End Cancelable Finger Vein Network for Recognition

Yifan Wang, *Student Member, IEEE*, Jie Gui, *Senior Member, IEEE*, Yuan Yan Tang, *Life Fellow, IEEE*, and James Tin-Yau Kwok, *Fellow, IEEE*,

**Abstract**—Finger vein recognition technology has become one of the primary solutions for high-security identification systems. However, it still has information leakage problems, which seriously jeopardizes user’s privacy and anonymity and cause great security risks. In addition, there is no work to consider a fully integrated secure finger vein recognition system. So, different from the previous systems, we integrate preprocessing and template protection into an integrated deep learning model. We propose an end-to-end cancelable finger vein network (CFVNet), which can be used to design an secure finger vein recognition system. It includes a plug-and-play BWR-ROIAIAlign unit, which consists of three sub-modules: Localization, Compression and Transformation. The localization module achieves automated localization of stable and unique finger vein ROI. The compression module losslessly removes spatial and channel redundancies. The transformation module uses the proposed BWR method to introduce unlinkability, irreversibility and revocability to the system. BWR-ROIAIAlign can directly plug into the model to introduce the above features for DCNN-based finger vein recognition systems. We perform extensive experiments on four public datasets to study the performance and cancelable biometric attributes of the CFVNet-based recognition system. The average accuracy, EERs and  $D_{\leftrightarrow}^{sys}$  on the four datasets are 99.82%, 0.01% and 0.025, respectively, and achieves competitive performance compared with the state-of-the-arts.

**Index Terms**—Cancelable biomtrics, finger vein recognition, convolutional neural network, object localization, Plug-and-Play, template protection, security and privacy.

## I. INTRODUCTION

WITH the rapid development in the information society, traditional identification technologies based on password or ID card can no longer meet the security demand. In recent years, applications of biometrics in finance, security,

medical and other fields have shown many advantages [1]. Biometrics allows intelligent machines to automatically capture, process, analyse and recognize digital physiological or behavioral characteristic signals of the human body, and is at the forefront of artificial intelligence development. The main biometric features include face [2], fingerprint [3], veins [4] and gait [5]. As a representative technology for second-generation biometrics, finger vein recognition (FVR) has become the mainstream in recent research because of its convenience and higher security quality. It can be divided into several main steps: image acquisition, preprocessing, feature extraction and recognition. Deep learning based FVR systems can automatically complete the extraction and recognition steps. On the other hand, preprocessing, while being a key step in FVR [6], requires the design of special processing operations (such as region-of-interest extraction, image enhancement, and feature alignment) to suit the different acquisition devices and application scenarios. It can seriously affect the convenience, integrity, and automation level of the recognition system.

With biometrics being widely used, the information leakage problem can seriously jeopardize users’ privacy and anonymity [7]. Although biometrics is more difficult to be fraudulently copied or forged than traditional identification techniques, attackers can still track activities of subjects in different domains enrolled through biometrics [8]. Once a biometric feature is compromised, the system’s security will decrease drastically. This biometric feature can no longer be used, further limiting the number of biometric features that can be applied on a subject. As biometric information cannot be revoked and redistributed, Ratha et al. [9] proposed to solve this problem by introducing a concept called cancelable biometrics (CB), which is defined as a biometric signal that is subjected to an intentional and repeatable distortion transformation operation. It allows the biometric templates to be authenticated in the protected domain to achieve biometrics protection. According to the ISO/IEC 24745 standard on biometric information protection [10], a properly cancelable biometric should have the following attributes.

- **Irreversibility:** Given a protected template, it should not be possible to reconstruct the original biometric sample.
- **Revocability:** From a given biometric sample, it should be possible to issue multiple protected templates.
- **Unlinkability:** Given two protected templates that are generated by the same instances and stored in different systems, it should not be feasible to determine if they

This work was supported in part by the grant of the National Science Foundation of China under Grant 62172090; Start-up Research Fund of Southeast University under Grant RF1028623097. We thank the Big Data Computing Center of Southeast University for providing the facility support on the numerical calculations. (Corresponding author: Jie Gui.)

Y. Wang and J. Gui are with the School of Cyber Science and Engineering, Southeast University, Nanjing 210000, China. J. Gui is also with Engineering Research Center of Blockchain Application, Supervision and Management (Southeast University), Ministry of Education; Purple Mountain Laboratories, Nanjing 210000, China (e-mail: 230239767@seu.edu.cn, guijie@seu.edu.cn).

Yuan Yan Tang is with the Department of Computer and Information Science, University of Macao, Macao 999078, China (e-mail: yy-tang@um.edu.mo).

James Tin-Yau Kwok is with the Department of Computer Science and Engineering, The Hong Kong University of Science and Technology, Hong Kong 999077, China (e-mail: jamesk@cse.ust.hk).

This manuscript has been accepted by IEEE Transactions on Information Forensics & Security, DOI: 10.1109/TIFS.2024.3436528

belong to the same subject.

- **Performance:** The system's recognition performance should not be significantly degraded when using the biometric template protection, and should not be sensitive to the parameters of the template protection step employed.

Unlike traditional recognition methods, FVR systems based on deep convolutional neural network (DCNN) do not need to save the feature templates into a database, and thus there is no risk that the templates will be stolen [11]. However, an attacker can hack into the finger vein system to analyze the finger vein information output by the network. A main component of the DCNN is the convolutional operation, and one can recover the original vein template to some extent via deconvolution [12]. This can become a security risk for the DCNN-based FVR system once the template is recovered. To solve these problems, researchers combine biometric template protection with DCNN-based FVR system to design more secure systems. Using simple and effective irreversible transformations to reorganize or distort the biometric features, the CB template protection is designed to make it impossible for the attacker to restore the original features using the protected template. However, the template protection scheme proposed in previous works [12] requires first transforming the raw feature templates, and then they can be used as inputs to a DCNN-based recognition system. Similar to the preprocessing task, the template protection task is also separated from the DCNN model, which makes it impossible to realize a DCNN-based end-to-end recognition system.

To solve the above problems and achieve integrated finger vein recognition, we propose an end-to-end cancelable finger vein network CFVNet for efficient and secure recognition system. By directly inputting the finger vein images obtained from the collection device into the recognition system, we integrate preprocessing, feature extraction, template protection and recognition into a complete deep learning model.

The proposed system has a block warping remapping ROI align (BWR-ROIAlign) plug-and-play module, which consists of three sub-modules: localization, compression, and transformation. The localization sub-module localizes stable and unique regions in the same instances. This is important because finger vein feature maps extracted by a standard DCNN are sparse. For feature transformation-based biometric template protection, slight translation or rotation of the same instances can show obvious intra-class differences in the transformed feature template. The stable regions extracted by the localization sub-module allow feature alignment to effectively narrow intra-class differences. This approach can be regarded as an effective solution to automated finger vein image ROI localization.

For the compression sub-module, firstly, the spatial redundancy in the vein images is removed according to the ROI coordinates, and the unique stable finger vein ROI is retained. As the finger vein pattern is relatively simple, a standard DCNN may then produce redundant feature channels which increases the computational burden. As the key information may only exist in a small number of feature channels, the compression sub-module removes redundant spatial regions and feature channels by linear weighted fusion.

Finally, the transformation sub-module re-divides the compact feature maps into same-sized blocks in the source domain, and then randomly samples part of the blocks, maps them to the new feature maps in random order, and uses mesh warping to dilute the response connection between the boundary pixels in the blocks. The transformation sub-module completes the conversion of source domain features to protected domain features, extract and analyze the protected domain features, and finally use the transformed features to complete the identification in the protected domain. This introduces unlinkability, irreversibility and revocability with higher security to the identification system.

The major contributions of this paper are as follows.

- We propose an end-to-end cancelable finger vein network (CFVNet) for the FVR system. To the best of our knowledge, this is the first study that integrates finger vein image preprocessing, template protection, and recognition tasks into a complete DCNN model.
- We design a novel block warping remapping ROI align (BWR-ROIAlign) module, which consists of three sub-modules: localization, compression and transformation. The localization module automatically locates and extracts stable and unique finger vein ROIs. The compression module improves efficiency of the recognition system by reducing spatial and channel redundancies. The transformation module introduces unlinkability and irreversibility to the biometric recognition system. The BWR-ROIAlign module is a plug-and-play architectural unit.
- This is the first work to label finger vein ROIs. We label ROIs in four publicly available datasets, and conduct comprehensive experiments on these datasets to verify the recognition and localization performance of the proposed model. We also conduct analysis on unlinkability, revocability, and irreversibility of the CFVNet-based FVR system.

The rest of the paper is organized as follows. Section II briefly reviews the related works. Section III introduces the proposed CFVNet for FVR. Section IV presents the experimental setup, results, and analysis. Finally, the paper concludes with Section V.

## II. RELATED WORK

In this section, we briefly review the work related to FVR and cancelable finger vein biometrics.

### A. Finger Vein Recognition

FVR has four main steps: image acquisition, preprocessing, feature extraction and recognition. In the past decade, many effective solutions have been proposed for the recognition task. These methods can be categorized as using manual features [4] or deep learning [13]. In early FVR research, vein features (mainly based on the vein pattern, orientation or details) are usually produced manually by feature engineering. Miura et al. proposed the maximum curvature [14] and repeated line tracking [15] to manually extract vein features. Some common gradient operators, such as LBP, LDP, ELBP, Gabor filter [4]

and SIFT, are also used for vein feature extraction. Methods such as PCA, LDA, and Dictionary Learning [16] perform spatial projection and then map the high-dimensional images to low-dimensional vein features.

Recently, the outstanding performance of DCNN in various image processing tasks has attracted extensive attention from FVR researchers. Many recognition schemes have been proposed. Razdi et al. [17] first introduce the DCNN into FVR and designed a four-layer DCNN. Subsequently, researchers have proposed solutions to the problems associated with finger vein images, such as poor image quality, finger displacement/rotation, and complex background [6]. These include model structure design [13], data augmentation [18], attention mechanism [19], loss function [20], learnable feature descriptors [21] and other more advanced models [22]. These works can effectively improve performance of the FVR system, but they all require some preprocessing. For example, one has to use ROI extraction to locate a target region with stable and unique vein pattern features.

A detailed review on finger vein ROI extraction has been studied in our previous work [23]. Finger vein ROI extraction methods can be categorized into four types: (i) fixed window-based methods, (ii) thresholding-based methods, (iii) gradient operator based methods, and (iv) fine edge detection based methods. All these methods have drawbacks. For fixed window-based methods, the window size is usually fixed, and cannot adapt to changes. For thresholding and gradient operator based methods, the pixel values of the finger region have to be higher or lower than those in the background. However, in practice, the finger region pixel values can have a similar distribution as the background region due to lighting conditions and/or devices. Moreover, many operators are very sensitive to noise. As different devices acquire background region images with large differences in the noise distribution, it is easy to take the noise as the maximum response and detect the wrong edges, causing poor robustness. The fine edge detection methods are mainly customized for different devices and application scenarios, and cannot be easily applied to the other devices. The above problems lead to a separation of preprocessing tasks from the other tasks in deep learning based recognition systems, and affects the design and implementation of an integrated FVR framework.

### B. Cancelable Finger Vein Biometrics

Compared to the other FVR tasks, research on template protection is still relatively scarce. Existing template protection techniques can be mainly categorized into two types [24]: biometric cryptosystem and feature transformation (cancelable transformation) based methods. Biometric cryptosystem use biometric templates to protect the key or generate the key directly from biometric features. Depending on how the auxiliary data is obtained, these methods can be further categorized as key-binding or key-generation. Key-binding methods use a biometric-independent external key-binding biometric to obtain auxiliary data; while key-generation methods generate the auxiliary data from a biometric template and the key is produced directly from the auxiliary data and biometric template. In other words, biometric cryptosystem uses the finger

vein image in the source domain, which makes the system vulnerable to linkage attacks. Once the finger vein feature template is compromised, security of the system decreases drastically. This feature template can no longer be used, further limiting availability of the biometric features.

For feature transformation based methods, they generate the protected template  $T_P$  by transforming the original template  $T$  into another domain by a random key  $K$  and transformation function  $F$ . Only the transformed template is used for recognition. When the template is compromised, one only needs to change the key and regenerate the protected template. Feature transformation based methods are categorized as reversible and irreversible, depending on whether the transformation process is reversible or not. The reversible transformation is also known as salting or bio-hashing, which is performed by defining an orthogonal random transformation function using a key, through which the bio-features are transformed and further binarized sequences are matched. Shao et al. [25] perform randomization and chaotic scrambling of finger vein features to disrupt the positional distribution of pixels, and binarize the chaotic features to get the protected feature vectors. Ren et al. [12] encrypt finger vein images using RSA and use the encrypted images to train a CNN model for recognition. Liu et al. [26] use random projection to transform the finger vein detail point features to get the protected template, and use a deep belief network as discriminator to design the recognition system. Simon et al. [27] propose a template protection scheme without alignment. They design an efficient binary feature vector representation and utilize IoM hashing to obtain the protected feature vector. Shahreza et al. [28] apply bio-hash to generate protected templates from depth features of a deep learning model. Non-reversible transformation is first proposed and applied to fingerprint template protection by Ratha [9]. It uses a parametric adjustable invertible transformation of biometric features to obtain a protected template which cannot be recovered from the original template. Kauba et al. [8] test three transformation methods for generating revocable templates and study the impact of the different methods on recognition performance, renewability, unlinkability and irreversibility. Yang et al. [29] use a binary decision diagram (BDD) to create irreversible templates, and utilize the feature templates in conjunction with an ML-ELM to construct a revocable irreversible FVR system. Debiassi et al. [30] use an external key to change the gray value of an image, and achieve cancelable irreversible template generation in the image source domain.

Unlike previous FVR systems, in this paper, we integrate preprocessing and template protection into a deep learning model. The vein feature information during the recognition process is highly irreversible, unlinkable and cancelable. This improves FVR system's cancelable biometric attributes. Moreover, the proposed BWR-ROIAlign is a plug-and-play module for DCNN-based FVR systems, and thus provides a novel approach for secure and end-to-end design of FVR systems.

## III. METHODOLOGY

As mentioned in Section I, existing works do not consider integrating individual tasks in FVR into a deep learning model.

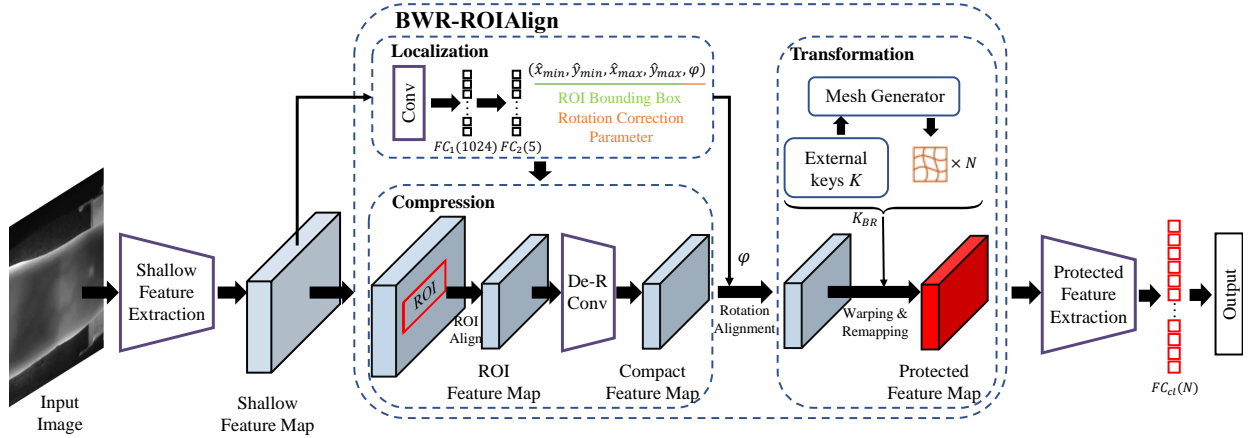


Fig. 1. Cancelable finger vein network (CFVNet) overall architecture. Localization, Compression and Transformation represent the three sub-functional modules of the BWR-ROIAlign. De-R Conv is the de-redundant convolution. External key  $K$  is the pseudo-random token generated during user registration.

In order to improve the integrity of a FVR system, we propose a novel cancelable finger vein network for FVR. Fig. 1 shows the overall architecture. In this section, we introduce the proposed model in detail. First, we introduce the overall design and functionality of the proposed CFVNet. Second, we introduce the proposed BWR-ROIAlign module. Finally, we introduce details of the three sub-modules of BWR-ROIAlign.

#### A. Cancelable Finger Vein Detector Architecture

Existing cancelable finger vein feature recognition systems perform template protection and recognition separately. Usually, the original templates are first converted to the protection domain and then stored to a database, which are subsequently transmitted or put into the classifier for recognition. The original feature templates often need to be designed with fine pre-processing, including ROI extraction and feature alignment. This makes the cancelable FVR system cumbersome.

The proposed CFVNet is shown in Fig. 1. Its skeleton is the ResNet50, which has been commonly used in classification tasks. The model is divided into two parts based on processing vein features from different domains: shallow feature (source domain) extraction, and deep feature (protected domain) extraction. The shallow feature extraction includes a convolutional layer (with  $7 \times 7$  kernels, stride 2, padding 3 and 64 channels), a batch normalization layer, and then ReLU activation, a max-pooling layer (with  $3 \times 3$  kernels, stride 2, and padding 1). The protected feature extraction sub-module has the same structure as layers 1 to 4 in the ResNet50, and has an average pooling layer with  $2 \times 2$  kernels. The numbers of channels in these layers are 24, 48, 72 and 96, respectively. In the final classification layer, the protected features are fed to a fully-connected layer. Its output is normalized by softmax that transforms it to a probability distribution for each class.

Similar to the popular two-factor biometric recognition system [31], each user has a key which represents an unique tokenized pseudo-random feature transformation. This key is then used in the transformation sub-module to apply an unique template protection transformation. The source domain features are converted to the protected feature map in the pro-

tection domain. Finally, the extracted protected feature vector is fed into the fully connected layer for recognition.

#### B. Block Warping Remapping ROI Align Module

The BWR-ROIAlign module includes three sub-modules: localization, compression and transformation. The localization module performs automated localization of stable and unique finger vein ROIs and predicts the rotational correction parameters. The compression module performs feature alignment and improves efficiency of the recognition system by reducing channel redundancy. The transformation module introduces unlinkability, irreversibility and revocability to the FVR system. The proposed BWR-ROIAlign is a plug-and-play architectural unit. The detailed implementation of each sub-module is discussed in the following.

1) **Localization**: The finger vein feature maps obtained by DCNN extraction have strong responses in key discriminative regions, but weak in the other regions. This leads to sparse feature maps. Finger displacement between the same instances increases the template intra-class difference after feature transformation. Correct feature alignment is an effective way to reduce the intra-class difference. Existing deep learning based FVR systems usually use images after preprocessing (such as ROI extraction and image enhancement) as inputs to the model to improve recognition performance. In fact, the location of unique stable finger vein pattern regions is performing feature alignment. In general, finger vein image ROI extraction focuses on obtaining a segmentation reference line in the horizontal and vertical directions, which are determined by the minimum internal tangent of the finger edge and position of the finger joint cavity, respectively. Existing techniques [23] usually use gradient operators or threshold segmentation methods to acquire the finger edge or joint cavity position. However, these methods are not robust to different devices or complex noise.

Inspired by object detection and spatial transformer [32] techniques, we design a localization module (Fig. 2), which consists of a convolutional layer (with  $1 \times 1$  kernels, stride 2 and 4 channels), and two fully-connected layers. This

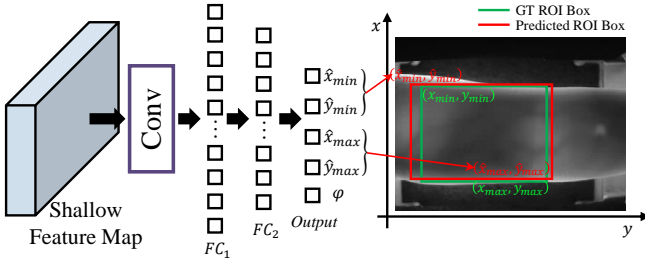


Fig. 2. ROI localization sub-module.

localization module is used to predict five parameters: four for the ROI coordinates and one for the rotation correction parameters  $\varphi$ . ROI coordinates localization is different from that in ordinary object detection tasks in that we can determine the number of ROIs. Therefore, the localization process does not require search discrimination of the target region. For object detection, bounding box regression finds a mapping  $f$  so that the offset between  $(\hat{P}_x, \hat{P}_y, \hat{P}_w, \hat{P}_h) = f(P_x, P_y, P_w, P_h)$  and the real bounding box  $(G_x, G_y, G_w, G_h)$  is reduced. For a set with  $N$  training pairs  $(P^i, G^i)_{i=1, \dots, N}$ , the loss is

$$Loss = \sum_{i=1}^n (t_*^i - \hat{\omega}_*^T \cdot F^i)^2, \quad (1)$$

where  $t$  is the offset between the regression target and the proposal,  $*$  denotes the four mappings (translation transformations  $\Delta x, \Delta y$ , and scale transformations  $S_w, S_h$ ), and  $F^i$  is the input feature map. To learn the various mappings, we minimize the following regularized least squares objective w.r.t. the learning parameter  $\omega$ :

$$W_* = \arg \min_{\omega_*} \sum_{i=1}^n (t_*^i - \hat{\omega}_*^T \cdot F^i)^2 + \lambda \|\hat{\omega}_*\|^2, \quad (2)$$

where  $\lambda$  is a regularization parameter.

General object detection tasks use the above method to realize regression to the bounding box, and consider the sensitivity of small objects to the coordinate offset. The MS COCO dataset uses the absolute size, and defines small objects as those smaller than  $32 \times 32$  pixels. Empirically, we find that the finger vein image ROIs are not small objects. Hence, we do not need to learn the four bounding box mappings. Instead, we can directly predict the real coordinates. The loss objective in the localization sub-module is defined as

$$Loss_{roi} = \begin{cases} \frac{1}{2} \sum_{i=1}^N (C^i - \hat{\omega}_*^T \cdot F^i)^2 & \text{if } |C^i - \hat{\omega}_*^T \cdot F^i| < 1, \\ \sum_{i=1}^N |C^i - \hat{\omega}_*^T \cdot F^i| - \frac{1}{2} & \text{otherwise,} \end{cases} \quad (3)$$

where  $C$  is the true finger vein ROI coordinates  $(x_{min}, y_{min}, x_{max}, y_{max})$ , and  $\hat{\omega}_*^T \cdot F^i$  is the predicted ROI coordinates  $(\hat{x}_{min}, \hat{y}_{min}, \hat{x}_{max}, \hat{y}_{max})$  obtained from the feature map. Parameter  $\omega$  is learned by minimizing the regularized least-squares objective.

For rotation correction, assume that the cross section of finger approximately resembles a circle and that the captured vein is close to the finger surface [33]. We can use the following transformation [34] for rotation correction:

$$\begin{bmatrix} x' \\ y' \end{bmatrix} = \begin{bmatrix} \cos(\varphi) & -\sin(\varphi) \\ \sin(\varphi) & \cos(\varphi) \end{bmatrix} \begin{bmatrix} x \\ y \end{bmatrix}, \quad (4)$$

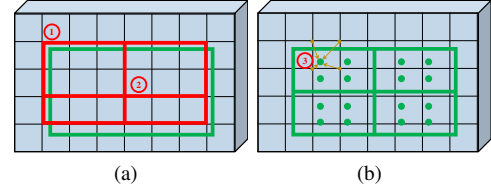


Fig. 3. Spatial redundancy removal without quantization loss. ① ROI coordinates mapped to corresponding grid cells on the feature map, ② divide the mapped grid cells into subregions of  $H \times W$  number, ③ Using linear interpolation in coordinate mapping and meshing.

where  $(x, y)$  is the coordinates of the input feature map, and  $(x', y')$  is the coordinates in the corrected feature map. Note that rotation correction is performed after compression (Section III-B2), and the localization module only predicts the rotation correction parameter  $\varphi$ .

More specifically, when a shallow feature map  $F$  of size  $(B, C, W, H)$  is used as input, the localization sub-module analyses the shallow feature information to get the ROI coordinates (of size  $(B, 4)$ ) and rotation correction parameters (of size  $(B, 1)$ ). The ROI coordinate is used in the compression module to remove spatial redundancy. The rotation correction parameter is used after the compression module to correct finger rotation.

2) **Compression:** Finger vein images have strong responses in critical discriminative regions but weak responses in the other regions, resulting in sparse feature maps. Moreover, for simple finger vein patterns, redundant feature channels increase the computational burden. Most feature channels include no or only a small amount of discriminative information, and the critical discriminative information exists only in a few feature channels. Therefore, we design the compression sub-module to remove spatial redundancy and channel redundancy.

a) *Spatial redundancy removal:* Finger vein pattern features are unique, but there are still unstable features (such as finger shape, position, device background, and environmental noise) in the images acquired by unconstrained acquisition devices. We combine the ROI coordinates  $(\hat{x}_{min}, \hat{y}_{min}, \hat{x}_{max}, \hat{y}_{max})$  obtained from the localization sub-module to extract dense and stable finger vein pattern feature regions on the shallow feature map, and unify them into a  $H \times W$  feature map (in the experiments,  $H = 32, W = 64$ ).

To extract specific regions in the feature map, a simpler approach is to map the ROI rectangular window coordinates to the corresponding grid cells on the feature map (Fig. 3-a ① operation). The mapped grid cells are then divided into  $H \times W$  sub-regions (Fig. 3-a ② operation). Finally, these sub-regions are sampled to obtain a uniformly-sized ROI feature map. However, non-vein regions in the finger vein feature map have low response, and so slight displacements in the sparse vein features can result in row or column variations. In particular, for block-based feature template transform methods, displacement variations can result in large intra-class differences. Therefore, proper template alignment is key to improving recognition performance of the protected system. We use linear interpolation (Fig. 3-b ③ operation) to avoid any quantization in coordinate mapping and meshing, and obtain

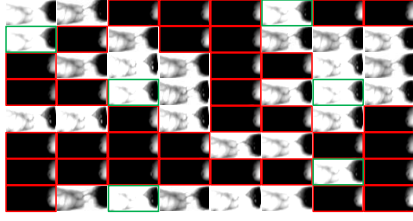


Fig. 4. Redundant feature map visualization. The green boxes contain little feature information, while the red boxes contain almost no feature information.

properly-aligned ROI features for subsequent sampling.

b) *Channel redundancy removal*: Redundant feature channels waste computational resources. Simple linear operations can reduce these redundant features. Fig. 4 visualizes the shallow feature maps after removing spatial redundancy. Some feature maps contain only a small amount of information, and some do not even have any. Simple linear fusion can effectively remove such redundant channels.

Inspired by group convolution [35], we divide the features into four groups and fuse each group, thereby reducing the redundant feature maps. Fig. 5 shows the De-Redundant Convolution (De-R Conv), which is divided into two paths. First, for a feature map  $F$  of size  $(B, C, H, W)$ , we use average pooling and two  $1 \times 1$  Conv to obtain the weight  $w$  and inverse weight  $w'$  of each channel (where  $w'$  is obtained by flipping  $w$ ). This operation is similar to channel attention. Weights  $w$  and  $w'$  are assigned to the corresponding feature maps to obtain  $F_w$  and  $F_{w'}$  (upper and lower parts of Fig. 6), respectively, which are the positively and negatively weighted paths. Divide  $F_w$  and  $F_{w'}$  into 4 groups, and linearly fuse them to get the feature maps  $F'_w$  and  $F'_{w'}$  of size  $(B, \frac{C}{4}, H, W)$  as

$$\begin{cases} F_w \Rightarrow \{F_w^1, F_w^2, F_w^3, F_w^4\}, \\ F'_{w'} = F_w^1 \oplus F_w^2 \oplus F_w^3 \oplus F_w^4, \end{cases} \quad (5)$$

where  $\Rightarrow$  denotes dividing the weighted feature maps equally into four groups of non-overlapping feature maps,  $\oplus$  denotes that the four groups of feature maps are linearly fused at the corresponding positions. Next, we feed  $F_w$  and  $F_{w'}$  into a  $3 \times 3$  convolution to extract the dense feature maps. Note that as  $w'$  is flipped for  $F_{w'}$  in the reverse-weighted path, feature maps with lower responses are given higher weights. However, they contain rich features in the forward-weighted path. Hence, we use a  $1 \times 1$  convolution to further compress them. Finally, the forward path has feature maps of size  $(B, \frac{C}{4}, H, W)$ , and the reverse path has feature maps of size  $(B, \frac{C}{8}, H, W)$ . The feature maps from both the forward and reverse paths are concatenated (of size  $(B, \frac{3C}{8}, H, W)$ ) and used as outputs. Before inputting the features to the transformation module, rotation correction of the vein features is performed using the rotation correction parameter.

3) *Transformation*: In an unprotected FVR system, an attacker can invade the database or analyze the network output of the finger vein information. In particular, for FVR systems based on DCNN, the main component of the DCNN is the convolution operation, and deconvolution can restore the operation to some extent and eventually restore the original

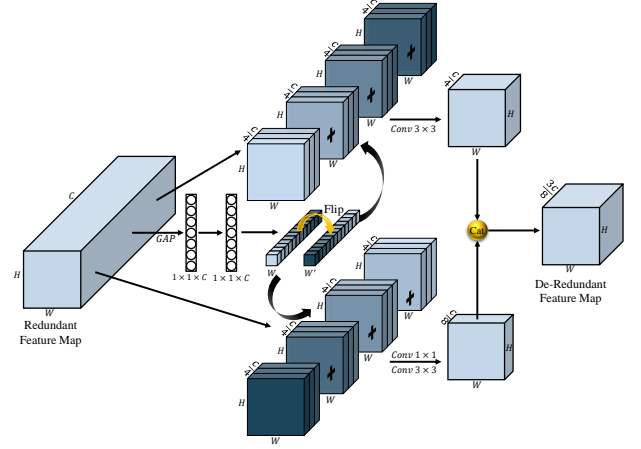


Fig. 5. De-R Conv Architecture. Here, + represents the positions summed.

feature template. This is the main security risk of DCNN-based FVR system. While we introduce feature transformation into the DCNN, the shallow features in the source domain are transformed to the protected domain by combining the user-defined external key, and the final identification of the user is performed in the protected domain. In BWR-ROIAlign, the transformation sub-module uses a block warping remapping (BWR) template protection method to realize the template transformation. This method is divided into two parts: block mesh warping and block remapping. It has four hyperparameters: image block size  $b$ , warping mesh size  $s$ , warping factor  $o$ , and resampling rate  $r$ . These parameters are system-level hyperparameters that are set prior to training the CFVNet, and are used to balance the recognition system's template protection attributes and recognition performance. The user's key corresponds to a unique tokenized pseudo-random feature transformation, which ensures that each user possesses a unique template protection transformation under the current parameter set, assuring accurate recognition.

Let the size of the source domain feature map  $F(x, y)$  be  $(H, W)$ . We divide  $F$  into  $b \times b$  pixel blocks:  $\{A_T\}$ , where  $T = 1, 2, \dots, HW/b^2$ . Each  $A_T$  is assigned an initial  $s \times s$  quadrilateral mesh  $G_T$ . The vertices of all meshes in  $G_T$  are then randomly transformed to obtain the warped mesh  $B_T$ . For any initial mesh, let  $(G_{xi}, G_{yi})$  be the coordinates of the  $i$ th vertex  $G_i$ . Similarly, let  $B_i$  be the  $i$ th vertex after the transformation, and  $(B_{xi}, B_{yi})$  be the coordinates after transformation. The coordinates are related as

$$\begin{cases} B_{xi} = G_{xi} + \Delta x \times o_x, \\ B_{yi} = G_{yi} + \Delta y \times o_y, \end{cases} \quad (6)$$

where  $\Delta x$  (resp.  $\Delta y$ ) is the length of single mesh in the  $X$  (resp.  $Y$ ) direction,  $o_x$  (resp.  $o_y$ ) is the warping factor in the  $X$  (resp.  $Y$ ) direction (and takes values in  $[0, o]$ ). The higher the warping degree, the closer is its value to 1, and vice versa.

After the vertices are transformed, all  $A_T$ 's are divided by randomly warped irregular meshes. These meshes are then mapped to the corresponding regular meshes of the new feature block  $C_T$ 's. Consider a given warped grid  $B_1B_2B_3B_4$  (with edges  $B_1B_2$ ,  $B_2B_3$ ,  $B_3B_4$  and  $B_4B_1$ ). These edges are

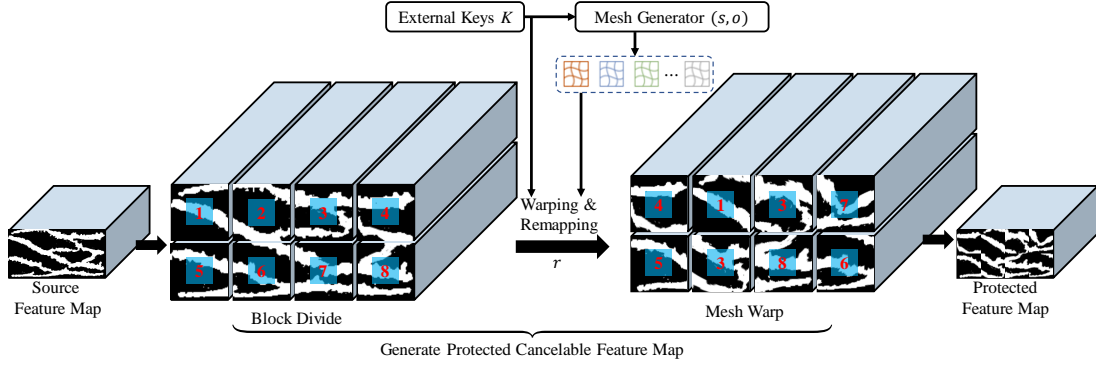


Fig. 6. Transformation sub-module.  $b$ : block size,  $s$ : mesh size,  $o$ : warping factor and  $r$ : resampling rate (In this work,  $b = 16$ ,  $s = 8$ ,  $o = 0.625$ ,  $r = 0.8$ ).

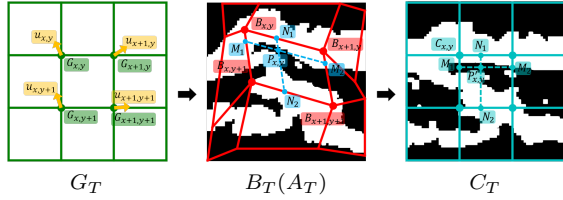


Fig. 7. Feature block warping.  $G_T$  is the initialized mesh,  $B_T(A_T)$  is the divided feature block with warped mesh, and  $C_T$  is the warped feature block.  $u_{x,y}$  is the transformation at vertex  $G_{x,y}$ , and warped vertex  $B_{x,y} = G_{x,y} + u_{x,y}$ ,  $u_{x,y}$  is a transformation in the vertex  $G_{x,y}$  as in Eq. 7.  $B_{x,y}B_{x+1,y}B_{x+1,y+1}B_{x,y+1}$  are the four vertices of a warped grid (abbreviated  $B_1B_2B_3B_4$  in the text).  $M_1M_2$  is the  $t_x$ th node line in the direction of  $B_{x,y}B_{x+1,y}$ ,  $N_1N_2$  is the  $t_y$ th node line in the direction of  $B_{x+1,y}B_{x+1,y+1}$ .  $P$  is the intersection of  $M_1M_2$  and  $N_1N_2$  in  $B_T(A_T)$ .  $P'$  is the point corresponding to  $P$  in  $C_T$ .

divided into  $t - 1$  equal parts.  $B_1B_2B_3B_4$  is divided into  $t \times t$  nodes. Similarly, a grid of the new feature block is also divided into  $t \times t$  nodes. Let  $M_1M_2$  be the  $t_x$ th node line in the direction of  $B_1B_2$ ,  $N_1N_2$  be the  $t_y$ th node line in the direction of  $B_2B_3$  (where  $t_x, t_y \in [0, t]$ ). Let  $P$  be the intersection of  $M_1M_2$  and  $N_1N_2$ . The coordinates  $(P_x, P_y)$  of  $P$  are

$$\begin{cases} P_x = M_{1x} + \frac{M_{2x} - M_{1x}}{t} \times t_x, \\ P_y = M_{1y} + \frac{M_{2y} - M_{1y}}{t} \times t_y, \end{cases} \quad (7)$$

where  $(M_{1x}, M_{1y})$  and  $(M_{2x}, M_{2y})$  are the coordinates of  $M_1$  and  $M_2$ , respectively. Next, the point  $P$  is mapped to the same position in the grid of the new feature block as point  $P'$ . The coordinates  $(P'_x, P'_y)$  of  $P'$  are

$$\begin{cases} P'_x = C_x + \Delta t \times t_x, \\ P'_y = C_y + \Delta t \times t_y, \end{cases} \quad (8)$$

where  $C$  is the top-left vertex of the grid of the new feature block,  $(C_x, C_y)$  are the coordinates of  $C$ , and  $\Delta t$  is the length between the two points in the new feature block after subdivision. Fig. 7 shows the feature block warping process. The  $C_T$ 's are sampled with a sampling rate  $r$ . A subset  $\{C'_T\}$  of  $\{C_T\}$  is selected to reconstruct the image, and  $\{C'_T\}$  is randomly mapped to the feature map  $F_E$  to produce the final

protected domain feature map (note that some blocks in  $\{C'_T\}$  will be reused) in the following way:

$$F_E = F_{map}(f_r(\{C_T\}, r), k), \quad (9)$$

where  $f_r(\cdot)$  denotes random sampling the warped image block,  $k$  is a user's key, and  $f_{map}(\cdot)$  denotes random sampling of the subset  $\{C'_T\}$  obtained after the operation of  $f_r(\cdot)$ , which is then mapped to generate the protected feature map  $F_E$ .

The transformation sub-module introduces unlinkability and irreversibility to the recognition system, which ensures that the subsequent feature extraction and recognition are performed in the protected domain. It should be noted that when training the CFVNet model, all users have unique and correct keys. When using the trained model for inference/recognition, enrolled users with the correct finger vein features and keys will get high confidence in recognition. Using non-enrolled user's finger vein features or incorrect key is considered an illegal attack, and the model will output very low confidence. Once the user's key is stolen, it is necessary to assign a new key to the user and retrain the CFVNet model for security.

## IV. EXPERIMENTS

In this section, the proposed CFVNet is used for FVR. We perform a number of experiments on multiple datasets. Section IV-A first describes the experimental setup, including the finger vein datasets, evaluation metrics and implementation details. In Section IV-B, ablation experiments are designed to validate effectiveness of BWR-ROIALign. Next, experiments are conducted to analyze the effectiveness of the three sub-modules in BWR-ROIALign on localization (Section IV-C), model size and FLOPS (Section IV-D), unlinkability, revocability and irreversibility (Section IV-E). Finally, in Section IV-F, we compare with various FVR works and shows the advantages of CFVNet in recognition and template protection.

### A. Experimental Setup

1) *Datasets*: Four datasets are used (i) SDUMLA-FV [36], a multimodal feature dataset from Shandong University, (ii) the UTFVP [37] dataset from the University of Twente, (iii) the FV-USM [38] dataset from the Universiti Teknologi Malaysia, and (iv) the HKPU-FV [39] dataset from the Hong Kong Polytechnic University. Table I shows the information

TABLE I  
DETAILS OF THE EXPERIMENTAL DATASETS.

Datasets	Subjects	Fingers	Capture times	Total images	Image size
HKPU-FV	250	6	12/6	3132	513×256pxl
SDUMLA-FV	106	6	6	3816	320×240pxl
UTFVP	60	6	4	1440	672×380pxl
FV-USM	123	4	6	5904	640×480pxl

of each dataset. Note that the finger vein image sizes in all datasets are normalized to  $256 \times 320$  (the images in FV-USM are first flipped to finger horizontally, and then centrally cropped to  $360 \times 480$ ).

2) *Evaluation Metrics*: To evaluate FVR performance, commonly used metrics include (i) false accept rate (FAR), which is the probability that the recognition system accepts a fake as enrolled user; (ii) false reject rate (FRR), which is the probability that the system rejects an enrolled user as a fake; (iii) equal error rate (EER), which is the point where FAR equals to FRR; and (iv) receiver operating characteristic (ROC) curve.

The localization performance is evaluated by intersection over union (IoU) [40], which is commonly used to measure the overlap between the predicted box and its true annotation:

$$IoU = \frac{Area\ of\ Overlap}{Area\ of\ Union}, \quad (10)$$

where *Area of Overlap* and *Area of Union* denote the intersection area and concatenation area of the prediction box and its true annotation, respectively.

Unlinkability of a cancelable recognition system is assessed based on the following global unlinkability metric [41]:

$$D_{\leftrightarrow}^{sys} = \int p(s|H_m)[p(H_m|s) - p(H_{nm}|s)]ds, \quad (11)$$

where  $s$  is the linkage score between two protected templates  $T_1$  and  $T_2$ . Based on the paired hypothesis  $H_m$  = “both templates belong to mated instances” and the unpaired hypothesis  $H_{nm}$  = “both templates belong to non-mated instances”, we obtain the conditional probabilities  $p(H_m|s)$  and  $p(H_{nm}|s)$ , for a given matching score  $s$ .  $p(s|H_m)$  is the conditional probability of obtaining a score  $s$  knowing that the two templates come from mated instances. A small  $D_{\leftrightarrow}^{sys}$  indicates that the link is weak, and vice versa.

Invertibility is evaluated by the pre-image attack match rate (P-IAMR) [42], which is defined as the acceptance rate of a protected system when accessed with the original biometric feature samples from a subject:

$$P-IAMR = \frac{1}{N} \sum_{i=1}^N \delta\{y_i = y_{gt}\}, \quad (12)$$

where  $N$  is the number of pre-image attacks,  $y_i$  is the predicted class label of the current attack sample, and  $y_{gt}$  is its corresponding true class label. The function  $\delta\{\text{condition}\}$  is 1 if the condition is satisfied, and 0 otherwise. A higher P-IAMR indicates a higher level of invertibility for the template.

The recognition system is revocable if the impostor and pseudo-impostor distributions overlap and the genuine and pseudo-impostor distributions are clearly distinguishable. The

degree of overlap between two distributions can be measured using the *decidability index*  $d'$ , which reflects the revocability of the recognition system [43]. This metric is described as the normalized distance between the means of the two distributions. For two distributions with means  $\mu_1$  and  $\mu_2$ , and standard deviations  $\sigma_1$  and  $\sigma_2$ , respectively,  $d'$  is defined as

$$d' = \frac{|\mu_1 - \mu_2|}{\sqrt{\frac{1}{2}(\sigma_1^2 + \sigma_2^2)}}. \quad (13)$$

A higher value of  $d'$  indicates good separation between the two distributions, and vice versa.

3) *Implementation details*: To train the CFVNet, we adopt Adam [44] as the optimizer (with a momentum of 0.9). The loss consists of the classification loss (cross-entropy loss) and regression loss (smooth  $\ell_1$  loss). The learning rate and batch size are set to 0.001 and 64, respectively. The CFVNet model is trained on two RTX 3090 GPUs, Intel Xeon(R) silver 4110 CPU@2.10GHz and 32GB RAM using the PyTorch framework for 200 training epochs. All datasets are divided into training and testing sets in the ratio of 8 : 2.

### B. Ablation Experiments

In this section, we perform ablation experiments on CFVNet. Five schemes are included 1) Directly using the raw images (size  $256 \times 320$ ) to train a standard DCNN; 2) Using manually ROI images (size  $128 \times 256$ ) to train a standard DCNN; 3) Perform spatial redundancy removal by activating only the localization sub-module in BWR-ROIAlign; 4) Fully activating the compression sub-module on top of scheme 3; 5) Activate the localization, compression and transformation sub-modules in BWR-ROIAlign module.

TABLE II  
COMPARISON AMONG ABLATION EXPERIMENTS RECOGNITION PERFORMANCE (%) OF THE FIVE SCHEMES ON EACH DATASET.

Scheme	HKPU-FV		SDUMLA-FV		UTFVP		FV-USM		Average	
	ACC	EER	ACC	EER	ACC	EER	ACC	EER	ACC	EER
1	97.89	0.10	91.90	1.50	61.94	5.56	<b>100</b>	<b>0.00</b>	87.93	1.79
2	98.66	0.08	91.35	1.89	75.28	4.31	99.89	0.0002	91.30	1.57
3	98.66	0.17	95.79	0.68	80.56	2.96	<b>100</b>	<b>0.00</b>	93.75	0.95
4	98.66	0.15	96.46	0.51	84.72	2.04	<b>100</b>	<b>0.00</b>	94.96	0.68
5	<b>100</b>	<b>0.00</b>	<b>99.84</b>	<b>0.04</b>	<b>99.44</b>	<b>0.01</b>	<b>100</b>	<b>0.00</b>	<b>99.82</b>	<b>0.01</b>

Fig. 8 shows the ROC curves obtained on each dataset. It can be observed that CFVNet’s ROC curve is very close to the coordinate axis, and achieves very low EERs compared to the other schemes. Table II shows the recognition accuracy and EER obtained on each dataset. As can be seen, using manually extracted ROI images to train the standard DCNN improves the average recognition accuracy by 3.37% and reduces the average EER by 0.22% compared to Scheme 1. This is due to the fact that the feature information used for analysis and discrimination in the extracted ROI finger vein image is more stable, and the complex background noise of finger shape, position or device is removed. These reduce the difference between the same instances to some extent. In Scheme 3, we activate the localization sub-module in BWR-ROIAlign and activate spatial redundancy removal in the compression

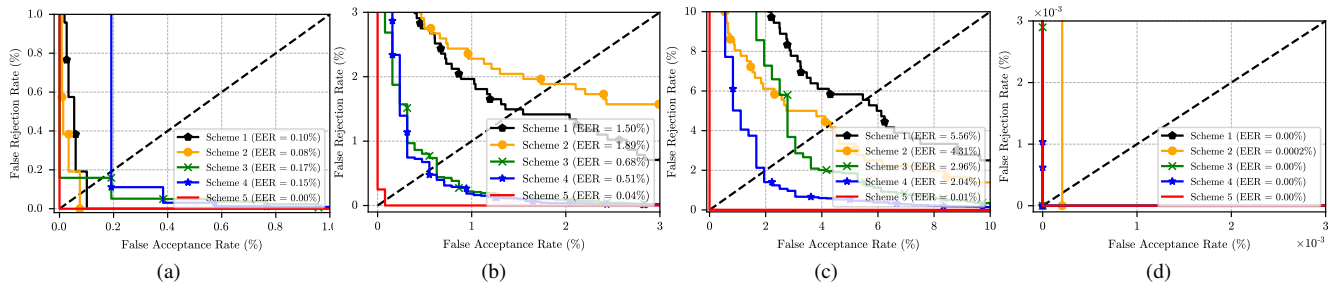


Fig. 8. Comparison of ablation experiment ROC curves for five schemes on each dataset. (a) HKPU-FV (b) SDUMLA-FV (c) UTFVP (d) FV-USM

 TABLE III  
 COMPARISON AMONG ROTATION CORRECTION EFFECTS.

	HKPU-FV		SDUMLA-FV		UTFVP		FV-USM	
	ACC	EER	ACC	EER	ACC	EER	ACC	EER
CFVNet-L*	98.85	0.38	94.97	0.79	78.33	4.17	100	0.0002
CFVNet-L	98.66	0.17	95.79	0.68	80.56	2.96	100	0.0
CFVNet-S*	98.66	0.19	95.13	0.55	77.78	2.78	99.80	0.0
CFVNet-S	98.66	0.15	96.46	0.51	84.72	2.04	100	0.0
CFVNet*	100	0.0	99.37	0.06	98.61	0.02	100	0.0
CFVNet	100	0.0	99.84	0.04	99.44	0.01	100	0.0

\* No regression on  $\varphi$  and no rotation alignment was performed.

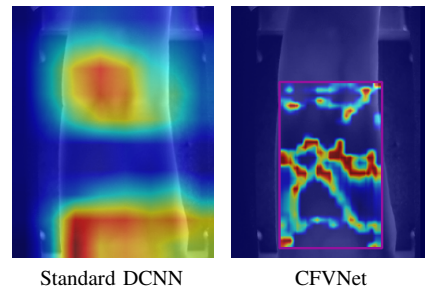


Fig. 9. Standard DCNN and CFVNet-based class activation maps.

sub-module. The average recognition accuracy is improved by 2.45% and the average EER is reduced by 0.62% compared with Scheme 2. Unlike manual ROI extraction which achieves hard alignment of the stable regions, the localization sub-module can be seen as soft feature alignment. Benefiting from the correction of the recognition branch, the localization branch's parameters are optimized towards the smallest differences in the same instances (which also explains why the proposed model is not the most compatible approach with manually labelled regions among other ROI-localizable DCNN models). Scheme 4 improves the average recognition accuracy by 1.21% and reduces the average EER by 0.27% while reducing nearly 4/5 of the parameters. In Scheme 2, although spatial redundancy is removed to make the analysis discriminant region more stable, there are still unstable tissue features around the vein, and the redundant feature channels may overly focus on changes in these regions. Using De-R Conv in the compression sub-module to remove the redundant channels allows the model to focus more on the vein pattern information. In Scheme 5, the transformation sub-module completes the transformation from source-domain features to protected-domain features, and then extract and analyze the protected-domain features, finally completing the recognition process in protected-domain by using the transformed features. Usually when a biometric template is protected, the biometric information contained in the template (such as vein branches, intersections, and branching angles) is destroyed due to the transformation operations. The recognition system performance, which use protected templates, decreases dramatically. However, comparing with the baseline model, the average recognition accuracy of CFVNet is improved by 11.89% and the average EER is reduced by 1.78%. This is due to the powerful learning ability of DCNN. Traditional recognition

systems based on manual processing of features is unable to deal with this abstract transformation, while the deeper convolutional layer in CFVNet learns the feature mapping rules in the transformation sub-module. This allows CFVNet to have significantly improved performance.

### C. Localization Performance Analysis

In this section, we study the CFVNet-based recognition system using class activation maps (CAM) [45] and localization performance. Fig. 9 compares the CAMs obtained on training a standard DCNN and CFVNet using raw images. When the raw image is used for recognition (Fig. 9, left), the model focuses on the feature information in the whole image (including device background, finger position or shape, surrounding tissue region and vein pattern). However, the feature region used for discrimination is fuzzy and unstable, and even non-vein region features are utilized for classification. After using the BWR-ROIAlign module through localization and compression (Fig. 9, right), unstable noise due to the device and acquisition environment is removed, and compressing the redundant channels allows the model to focus more on the vein pattern information rather than the other surrounding tissues.

Table IV shows the localization effect. CFVNet-L, CFVNet-S and CFVNet correspond to Schemes 3-5 in Section IV-B, respectively. As can be seen, the average IoUs are 89.53, 89.02 and 89.09, respectively. Common object detection models can obtain high IoUs due to their excellent object searching abilities. However, classification confidence tends to be low because these models mainly look for objects that may exist in the image. This is not suitable for the task of identification (due to low classification confidence, which leads to high FAR and FRR). In CFVNet, due to the penalty of the recognition branch

TABLE IV  
COMPARISON LOCALIZATION PERFORMANCE ON EACH DATASET.

Model	IoU			
	HKPU-FV	SDUMLA-FV	UTFVP	FV-USM
Faster RCNN	91.66	92.34	85.12	91.74
SSD300	90.74	93.12	91.24	94.19
CFVNet-L	86.36	90.74	87.72	93.31
CFVNet-S	86.83	90.06	85.95	93.23
CFVNet	85.45	89.73	86.33	84.85

TABLE V  
COMPARISON AMONG GFLOPs, PARAMS AND INFERENCE TIME.

Model	GFLOPs	Params (M)	Time (ms)	ACC (%)	EER (%)
MobileNet	1.48	<b>4.97</b>	16.33	56.92	5.69
ResNet50	6.62	24.73	16.84	87.93	1.79
EfficientNet-B7	34.66	65.32	52.52	96.73	0.35
VIT	39.86	203.36	15.92	69.42	5.88
SSD300	34.86	35.64	103.86	89.42	48.17
Faster RCNN	167.98	41.76	34.56	92.32	43.73
CFVNet-L	2.70	38.58	<b>14.39</b>	93.75	0.95
CFVNet-S	<b>0.35</b>	8.46	15.24	94.96	0.68
CFVNet	<b>0.35</b>	8.46	31.26	<b>99.82</b>	<b>0.01</b>

to feature alignment in the localization branch, the ROI is aligned towards the smallest differences in the same instances instead of manually labeling the regions. This further proves that the localization sub-module is a soft feature alignment scheme. Similarly, this soft alignment is compatible with the more refined feature alignment required by the feature transformation during the source to protected domain.

D. Model Size and Runtime Analysis

Table V compares mainstream classification models and CFVNet models in terms of GFLOPs, number of parameters (Params), inference time and average recognition performance (the number of classes is 600). Except MobileNet model that cannot achieve effective recognition task, the proposed CFVNet has the smallest number of model parameters and the lowest computational consumption. Moreover, the recognition performance is significantly improved compared with the other models. CFVNet-L takes the least inference time compared with the other models, and CFVNet-S reduces the parameters by 4/5 by non-destructively removing the redundant feature channels. The inference time is increased only by 0.74 ms. In CFVNet, the transformation of the vein feature source domain to the protected domain is achieved by utilizing a feature cancelable transformation proposed in the transformation sub-module. In template protection tasks, this operation usually requires more time. The feature maps obtained in DCNN are usually high-dimensional, which further increases the burden of the transformation sub-module. Hence, we remove the redundant feature channels by the compression sub-module, so as to keep CFVNet’s inference time to be relatively small and still improve recognition efficiency.

E. Unlinkability, Revocability and Irreversibility Analysis

In this section, we evaluate the template protection attributes and security of the CFVNet-based FVR system on four datasets and their mixed datasets. We consider both the normal scenario and the stolen scenario. In the normal scenario, which

TABLE VI  
GLOBAL LINKABILITY ( $D_{\leftrightarrow}^{sys}$ ) IN THREE SCENARIOS ON EACH DATASET.

Scheme	HKPU-FV	SDUMLA-FV	UTFVP	FV-USM	MIX-D
1	0.028	0.026	0.022	0.025	0.014
2	0.162	0.155	0.168	0.061	0.199
3	0.238	0.179	0.228	0.129	0.250

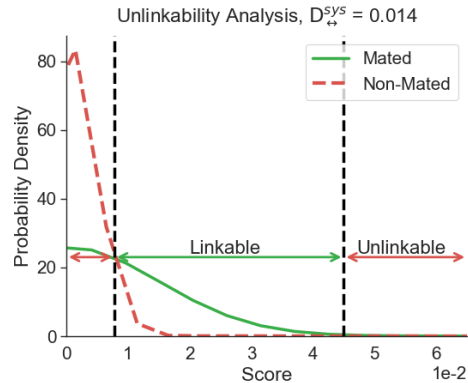


Fig. 10. Normal scenario unlinkability analysis on MIX-D.

is the expected scenario for most cases, the hyperparameter settings and the user’s key are considered secret and not disclosed. However, in the stolen scenario, the attacker (impostor) has the system’s hyperparameters and/or the enrolled user’s key to access the system in combining with the unenrolled finger vein template. The following three scenarios are considered. 1) Normal scenario, where the attacker does not have any information about the recognition system and accesses the system using an unenrolled template. 2) Transformation sub-module hyperparameters are stolen, where the attacker has the transformation sub-module hyperparameters of the target recognition system, and uses the hyperparameters to randomly generate a key to access the system combining with an unenrolled template. 3) The enrolled user’s key is stolen, where the attacker has the enrolled user’s right key and accesses the system combining with an unenrolled template. These scenarios pose gradually increasing security risks from 1 to 3. Based on these three scenarios, the template protection attributes and security of the CFVNet-based finger vein recognition system are further analyzed.

Protected templates generated using different keys are unlinkable, which makes it possible to set up different keys to produce unlinkable protected templates when the user is enrolled in multiple applications. So we set five random keys for each instance to cross matching, record the mated scores and non-mated scores, and compute the global linkability  $D_{\leftrightarrow}^{sys}$ . It should be noted that during the evaluation process, in the normal scenario these keys are random keys generated under random hyperparameters, in scenario 2 the hyperparameters are stolen, which means that these keys are random keys generated under the hyperparameters of the target recognition system, and in scenario 3 the keys have been stolen and these keys are the correct keys of the enrolled users.

Table VI shows the global linkability metric  $D_{\leftrightarrow}^{sys}$  on each

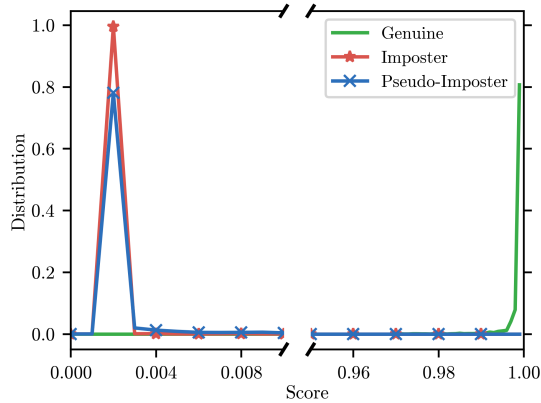


Fig. 11. In normal scenario, The Genuine, Imposter and Pseudo-Imposter distribution on MIX-D.

dataset. In the normal scenario, the CFVNet-based finger vein recognition system presents minimal linkability and satisfies the CB requirement for unlinkability. In Scenario 2, when the system hyperparameters are stolen, linkability between the cross-systems slightly increases. In Scenario 3, the attacker has the enrolled user’s key, linkability between the cross-systems increases and shows some linkability. As can be seen from Fig. 10, there is considerable overlap between the mated and non-mated instance score distributions, which means that they have essentially the same distribution and are impossible to distinguish. Only when the mated scores are larger than the non-mated scores, the recognition system has minimal linkage shown in less than 3.7% area.

Once a biometric is compromised, security of the recognition system decreases drastically. Cancelable biometrics ensure that templates generated using different keys are completely new. In other words, in CFVNet, the original (stolen) and new (regenerated) templates are generated from the same instances but the two templates are not linked. Revocability can empirically investigate this guarantee by generating the pseudo-impostor distribution. Similar to the evaluation of unlinkability, we set five random keys for each instance to cross matching. Cross-system impostor distributions are denoted as pseudo-impostor distributions. Revocability can be empirically validated if (1) the impostor and pseudo-impostor distributions overlap, and (2) the genuine and pseudo-impostor distributions have clear separability [43]. The genuine, impostor and pseudo-impostor scores distributions for MIX-D are shown in Fig. 11. There is a large overlap between the impostor and pseudo-impostor score distributions, whereas the genuine and pseudo-impostor scores are clearly distinguished. The separability or overlap between two distributions can be quantitatively estimated by the *decidability index*  $d'$ . Table VII shows the  $d'$  values between the three distributions on each dataset for different scenarios. In the normal scenario, the genuine score distribution is clearly distinguishable from the impostor and pseudo-impostor scores, while the impostor and pseudo-impostor score distributions highly overlap, which means that different protected templates generated from the same instances are similarly characterized to the inter-class

TABLE VII  
DECIDABILITY INDEX ( $d'$ ) BETWEEN THE THREE DISTRIBUTIONS FOR THE THREE SCENARIOS ON EACH DATASET.  $d'_{GI}$ ,  $d'_{GP}$  AND  $d'_{IP}$  ARE THE DISCRIMINABILITY INDICES BETWEEN GENUINE/IMPOSTOR SCORE DISTRIBUTIONS, GENUINE/PSEUDO-IMPOSTOR SCORE DISTRIBUTIONS AND IMPOSTOR/PSEUDO-IMPOSTOR SCORE DISTRIBUTIONS.

Scheme	1	2	3	
HKPU-FV	$d'_{GI}$	501	501	501
	$d'_{GP}$	2.84	1.87	1.38
	$d'_{IP}$	0.36	0.84	1.19
SDUMLA-FV	$d'_{GI}$	26.42	26.42	26.42
	$d'_{GP}$	9.00	1.65	1.46
	$d'_{IP}$	0.27	0.89	1.04
UTFVP	$d'_{GI}$	10.47	10.47	10.47
	$d'_{GP}$	3.27	2.04	1.85
	$d'_{IP}$	0.34	0.75	0.89
FV-USM	$d'_{GI}$	57.28	57.28	57.28
	$d'_{GP}$	4.12	2.77	2.49
	$d'_{IP}$	0.26	0.41	0.50
MIX-D	$d'_{GI}$	63.71	63.71	63.71
	$d'_{GP}$	3.99	1.86	1.34
	$d'_{IP}$	0.21	0.82	1.22

template samples. The CFVNet-based recognition system satisfies revocability. In Scenarios 2 and 3, revocability is slightly compromised because the attacker has some information about the recognition system, but the revocability requirement is still satisfied. Therefore, when the recognition system is attacked or damaged, a new recognition system can be trained by re-issuing new hyperparameters and keys.

Irreversibility of the CFVNet-based recognition system is analyzed through both the BWR template protection method and DCNN. In the BWR method, block remapping is reversible in the ideal case. This can be done by determining whether the block has been set to the correct position based on an indicator, and such a task is essentially like solving a square jigsaw puzzle. If we consider a brute-force attack against remapping that tries to rearrange them, the computational complexity is  $o(n!)$ . However, in the deep convolution of DCNN, most of the extracted feature maps are abstract semantic information, and the links between feature block boundaries are suppressed during DCNN feature extraction. This makes rearranging blocks by comparing the boundary similarity more difficult, with a computational complexity much larger than  $o(n!)$ . In addition, random warping is applied to the features within blocks and the available block boundary linkage distributions are further altered, further enhancing irreversibility of the recognition system. The resampling rate  $r$  in the transformation sub-module sets an upper bound on the reversible biometric information. The applied mesh warping can be considered irreversible because of the applied interpolation strategy, which leads to information loss. Therefore, it is impossible to fully recover the original data even if the distortion parameters are known. The deconvolution recovers the original biometrics by constructing valid training

TABLE VIII  
RECOGNITION PERFORMANCE OF CFVNET-BASED RECOGNITION SYSTEM ON NORMAL AND STOLEN SCENARIOS.

Scheme	HKPU-FV		SDUMLA-FV		UTFVP		FV-USM		MIX-D	
	ACC	EER	ACC	EER	ACC	EER	ACC	EER	ACC	EER
1	0.19	49.61	0.16	50.71	0.00	49.23	0.00	50.31	0.00	49.24
2	13.79	21.07	9.43	23.27	9.44	16.97	5.28	32.51	8.09	14.55
3	22.03	17.05	15.75	19.36	11.39	13.82	7.52	30.49	14.85	10.59

data, which is easily achieved in standard DCNN, whereas in protected CFVNet, the user and his/her original biometrics are not linked, and thus no valid training data can be constructed to train the deconvolution. When processing biometric features, DCNN-based recognition systems are deformed and compressed several times by multiple convolutional and nonlinear transformation layers (activation functions such as ReLU, pooling operations, etc.), which makes the input data be transformed into highly abstract feature representations. The nonlinear transformations also introduce information loss. Moreover, the DCNN-based recognition system only saves the model-trained weight parameters for recognition and does not additionally save any information about the biometric features, making it extremely difficult to recover the original biometric features.

We also evaluate the recognition performance of the CFVNet-based recognition system in three scenarios, as shown in Table VIII. In the normal scenarios, the attacker cannot access the recognition system. When the attacker steals system information, security of the FVR system is affected.

#### F. Comparison With SOTA Methods

In this section, we compare the proposed FVR system with state-of-the-art schemes. Tables IX and X compare the recognition accuracy and EER, respectively, of the latest FVR schemes on each dataset. The best results of the protected and unprotected schemes are shown in bold. As mainstream classification and detection models do not make special modifications for the FVR task, their recognition accuracies and EERs are not satisfactory. For example, MobileNet is hardly sufficient for basic recognition tasks in the presence of complex noise (HKPU-FV and SDUMLA-FV) or insufficient training data (UTFVP). Larger or more complex models, such as EfficientNet and Vision Transformer, require larger-scale training data or more learning epochs. As for the common object detection framework, it usually searches for possible objects in the input image. Even though it accomplishes the basic recognition task, the recognition confidence of a single object is low, leading to a recognition system with high FAR, FRR and EER, and is unsuitable for high-security recognition scenarios. The proposed CFVNet for FVR achieves an average recognition accuracy of 99.82% and an average EER of 0.01% on the four publicly available datasets. We also compare the CFVNet-based system’s global linkability with existing state-of-the-art schemes in Table XI. Combining localization performance analysis, model size, inference time and template protection attributes analysis, using CFVNet to design a cancelable FVR system outperforms existing models in terms

TABLE IX  
COMPARISON AMONG LATEST FINGER VEIN RECOGNITION SCHEMES RECOGNITION ACCURACY (%) ON EACH DATASET.

	Method	Year	HKPU-FV	SDUMLA-FV	UTFVP	FV-USM
Unprotected	MobileNet	2023	42.15	61.71	23.89	100
	ResNet50	2023	97.89	91.90	61.94	100
	EfficientNet-B7	2023	99.81	94.58	92.78	99.76
	Vision Transformer	2023	79.31	78.38	21.39	98.58
	SSD300	2023	90.04	93.40	74.44	99.80
	Faster RCNN	2023	97.31	95.68	77.50	98.78
	Das et al. [46]	2018	71.11	97.47	95.56	72.97
	Prasad et al. [47]	2018	97.81	92.37	91.97	99.88
	PLS-DA [48]	2022	-	97.52	-	99.86
	SSP-DBFL [49]	2023	99.39	99.07	-	99.40
	RGCN [6]	2023	-	98.04	92.22	100
	CFVNet-L (Ours)	2023	98.85	94.97	78.33	100
CFVNet-S (Ours)	2023	98.66	95.13	77.78	99.80	
Protected	BDD-ML-ELM [29]	2018	-	93.09	98.61	-
	Ren et al. [12]	2022	98.40	96.70	-	99.19
	Agerrahrou et al. [50]	2023	-	97.22	-	99.19
	<b>CFVNet (Ours)</b>	2024	<b>100</b>	<b>99.84</b>	<b>99.44</b>	<b>100</b>

TABLE X  
COMPARISON AMONG LATEST FINGER VEIN RECOGNITION SCHEMES EER (%) ON EACH DATASET.

	Method	Year	HKPU-FV	SDUMLA-FV	UTFVP	FV-USM
Unprotected	MobileNet	2023	7.26	4.44	11.04	0.00
	ResNet50	2023	0.10	1.50	5.56	0.00
	EfficientNet-B7	2023	0.002	0.71	0.69	0.0004
	Vision Transformer	2023	2.90	5.11	15.08	0.41
	SSD300	2023	49.06	45.97	49.70	47.96
	Faster RCNN	2023	45.37	42.64	44.69	42.20
	Kauba et al. [8]	2018	-	3.68	0.36	-
	PLS-DA [48]	2018	1.17	2.15	-	0.15
	FVFSNet [13]	2022	0.81	1.10	2.08	0.20
	FV-DGNN [22]	2023	1.43	0.67	-	-
	CFVNet-L (Ours)	2023	0.50	0.81	4.14	0.0002
	CFVNet-S (Ours)	2023	0.15	0.55	2.59	0.00
Protected	BDD-ML-ELM [29]	2018	-	7.04	-	-
	Shao et al. [25]	2022	2.68	-	-	1.72
	Zhang et al. [51]	2020	0.88	0.61	-	-
	Block Remapping [8]	2022	-	2.16	1.81	0.00
	Block Warping [8]	2022	-	3.50	0.32	0.15
	Bloom Filters [8]	2022	-	11.70	2.23	-
	Ren et al. [12]	2022	0.31	2.14	-	0.21
	GRP-DHI [52]	2022	0.38	0.61	-	-
	GRP-IoM [52]	2022	-	4.20	1.54	-
	Agerrahrou et al. [50]	2023	-	1.11	-	1.33
<b>CFVNet (Ours)</b>	2024	<b>0.00</b>	<b>0.04</b>	<b>0.01</b>	<b>0.00</b>	

of efficiency and performance. It can be seen that based on the proposed CFVNet model, an efficient, secure and end-to-end FVR scheme can be designed for critical applications. The vein feature information during the recognition process is highly irreversible, unlinkable and revocable, which effectively improved the template protection attributes of FVR system.

## V. CONCLUSION

Different from previous systems, we integrate preprocessing and template protection into a integrated deep learning model. We propose an end-to-end cancelable finger vein network. It can be used to design an efficient and secure finger vein recognition system. It includes a plug-and-play BWR-ROIAlign unit, which consists of three main sub-modules: localization, compression and transformation. The localization module realizes automated ROI localization, and benefits from the recognition branch to correct the whole model. The

TABLE XI  
COMPARISON AMONG LATEST FINGER VEIN TEMPLATE PROTECTION  
SCHEMES GLOBAL LINKABILITY  $D_{\leftrightarrow}^{sys}$  ON EACH DATASET.

Method	Year	HKPU-FV	SDUMLA-FV	UTFVP	FV-USM
ARH [27]	2020	-	-	0.052	-
Block Remapping [8]	2022	-	0.047	<b>0.016</b>	-
Block Warping [8]	2022	-	0.462	0.435	-
Bloom Filters [8]	2022	-	<b>0.019</b>	0.027	-
GRP-DHI [53]	2022	<b>0.020</b>	0.040	-	-
Aherrahrou et al. [50]	2023	0.030	-	-	0.027
CFVNet (Ours)	2024	<u>0.028</u>	<u>0.026</u>	<u>0.022</u>	<b>0.025</b>

parameters of the localization branch is optimized towards the smallest difference in the same instances to achieve optimal feature alignment, which is an effective feature soft alignment scheme. The compression module effectively removes unstable noise information through ROI position coordinates, and uses the proposed De-R Conv to losslessly and effectively remove a large number of redundant feature channels (reducing the number of parameters in the model by nearly a factor of 4/5). The transformation module uses the proposed BWR template protection method to introduce unlinkability, irreversibility and revocability to the system, which greatly improves the recognition system's template protection attributes. We performed experiments on four public datasets to study the performance and template protection attributes of the CFVNet-based system. The average accuracy, average EERs and average  $D_{\leftrightarrow}^{sys}$  on the four datasets can reach 99.82%, 0.01% and 0.025, respectively, and achieves competitive performance compared with the current state-of-the-art.

## REFERENCES

- [1] K. Shaheed, A. Mao, I. Qureshi, M. Kumar, and S. Hussain, "Recent advancements in finger vein recognition technology: methodology, challenges and opportunities," *Inform. Fusion*, vol. 79, pp. 84–109, 2022.
- [2] H. Yang, D. Huang, Y. Wang, and A. K. Jain, "Learning continuous face age progression: A pyramid of gans," *IEEE Trans. Pattern Anal. Mach. Intell.*, vol. 43, no. 2, pp. 499–515, 2019.
- [3] Y. Duan, J. Feng, J. Lu, and J. Zhou, "Estimating fingerprint pose via dense voting," *IEEE Trans. Inf. Forensics Security*, vol. 18, pp. 2493–2507, 2023.
- [4] C.-G. Ri, K.-I. Ri, and J.-H. Ri, "Robust and efficient finger vein recognition using binarized difference of gabor jet on grid," *IEEE Trans. Inf. Forensics Security*, vol. 18, pp. 177–189, 2022.
- [5] C. Fan, S. Hou, J. Wang, Y. Huang, and S. Yu, "Learning gait representation from massive unlabelled walking videos: A benchmark," *IEEE Trans. Pattern Anal. Mach. Intell.*, pp. 1–18, 2023.
- [6] Y. Wang, H. Lu, X. Qin, and J. Guo, "Residual gabor convolutional network and fv-mix exponential level data augmentation strategy for finger vein recognition," *Exp. Syst. Appl.*, vol. 223, p. 119874, 2023.
- [7] V. M. Patel, N. K. Ratha, and R. Chellappa, "Cancelable biometrics: A review," *IEEE Signal Process. Mag.*, vol. 32, no. 5, pp. 54–65, 2015.
- [8] C. Kauba, E. Piciucco, E. Maiorana, M. Gomez-Barrero, B. Prommegger, and P. Campisi, "Towards practical cancelable biometrics for finger vein recognition," *Inform. Sciences*, vol. 585, pp. 395–417, 2022.
- [9] N. K. Ratha, J. H. Connell, and R. M. Bolle, "Enhancing security and privacy in biometrics-based authentication systems," *IBM Syst. J.*, vol. 40, no. 3, pp. 614–634, 2001.
- [10] ISO Central Secretary, "Information security, cybersecurity and privacy protection — biometric information protection," International Organization for Standardization, Geneva, CH, Standard ISO/IEC 24745:2022, 2022. [Online]. Available: <https://www.iso.org/standard/75302.html>
- [11] J. Huang, M. Tu, W. Yang, and W. Kang, "Joint attention network for finger vein authentication," *IEEE Trans. Instrum. Meas.*, vol. 70, pp. 1–11, 2021.
- [12] H. Ren, L. Sun, J. Guo, C. Han, and F. Wu, "Finger vein recognition system with template protection based on convolutional neural network," *Knowledge-Based Syst.*, vol. 227, p. 107159, 2021.
- [13] J. Huang, A. Zheng, M. S. Shakeel, W. Yang, and W. Kang, "Fvfnnet: Frequency-spatial coupling network for finger vein authentication," *IEEE Trans. Inf. Forensics Security*, vol. 18, pp. 1322–1334, 2023.
- [14] N. Miura, A. Nagasaka, and T. Miyatake, "Extraction of finger-vein patterns using maximum curvature points in image profiles," *IEICE Trans. Inf. Syst.*, vol. 90, no. 8, pp. 1185–1194, 2007.
- [15] N. Miura, A. Nagasaka, and T. Miyatake, "Feature extraction of finger-vein patterns based on repeated line tracking and its application to personal identification," *Mach. Vision Appl.*, vol. 15, pp. 194–203, 2004.
- [16] L. Yang, X. Liu, G. Yang, J. Wang, and Y. Yin, "Small-area finger vein recognition," *IEEE Trans. Inf. Forensics Security*, vol. 18, pp. 1914–1925, 2023.
- [17] S. A. Radzi, M. K. Hani, and R. Bakhteri, "Finger-vein biometric identification using convolutional neural network," *Turk. J. Electr. Eng. Comput. Sci.*, vol. 24, no. 3, pp. 1863–1878, 2016.
- [18] G. Wang, C. Sun, and A. Sowmya, "Learning a compact vein discrimination model with generated samples," *IEEE Trans. Inf. Forensics Security*, vol. 15, pp. 635–650, 2019.
- [19] H. Qin, R. Hu, M. A. El-Yacoubi, Y. Li, and X. Gao, "Local attention transformer-based full-view finger-vein identification," *IEEE Trans. Circuits Syst. Video Technol.*, 2022.
- [20] B. Hou and R. Yan, "Arcvein-arccosine center loss for finger vein verification," *IEEE Trans. Instrum. Meas.*, vol. 70, pp. 1–11, 2021.
- [21] S. Li, R. Ma, L. Fei, and B. Zhang, "Learning compact multipresentation feature descriptor for finger-vein recognition," *IEEE Trans. Inf. Forensics Security*, vol. 17, pp. 1946–1958, 2022.
- [22] J. Chang, T. Lai, L. Yang, C. Fang, Z. Li, and H. Fujita, "Fv-dgmn: A distance-based graph neural network for finger vein recognition," *IEEE Trans. Instrum. Meas.*, vol. 72, pp. 1–11, 2023.
- [23] W. Yifan, L. huimin, G. Ruoran, and L. Yang, "Review: Region of interest extraction from finger vein images," *J. Comput. Eng. Appl.*, vol. 57, no. 13, 2021.
- [24] A. K. Jain, A. Ross, and U. Uludag, "Biometric template security: Challenges and solutions," in *Proc. Eur. Signal Process. Conf., EUSIPCO*. IEEE, 2005, pp. 1–4.
- [25] L. Shao, H. Ren, L. Sun, C. Han, and J. Guo, "Template protection based on chaotic map for finger vein recognition," *IEEE Trans. Electr. Electron. Eng.*, vol. 17, no. 1, pp. 82–95, 2022.
- [26] Y. Liu, J. Ling, Z. Liu, J. Shen, and C. Gao, "Finger vein secure biometric template generation based on deep learning," *Soft Comput.*, vol. 22, pp. 2257–2265, 2018.
- [27] S. Kirchgasser, C. Kauba, Y.-L. Lai, J. Zhe, and A. Uhl, "Finger vein template protection based on alignment-robust feature description and index-of-maximum hashing," *IEEE Trans. Biom. Behav. Identity Sci.*, vol. 2, no. 4, pp. 337–349, 2020.
- [28] H. O. Shahreza and S. Marcel, "Towards protecting and enhancing vascular biometric recognition methods via biohashing and deep neural networks," *IEEE Trans. Biom. Behav. Identity Sci.*, vol. 3, no. 3, pp. 394–404, 2021.
- [29] W. Yang, S. Wang, J. Hu, G. Zheng, J. Yang, and C. Valli, "Securing deep learning based edge finger vein biometrics with binary decision diagram," *IEEE Trans. Ind. Inf.*, vol. 15, no. 7, pp. 4244–4253, 2019.
- [30] L. Debiasi, S. Kirchgasser, B. Prommegger, A. Uhl, A. Grudzień, and M. Kowalski, "Biometric template protection in the image domain using non-invertible grey-scale transforms," in *Proc. Int. Workshop Inf. Forensics Secur., WIFS*. IEEE, 2019, pp. 1–6.
- [31] A. T. B. Jin, D. N. C. Ling, and A. Goh, "Biohashing: two factor authentication featuring fingerprint data and tokenised random number," *Pattern Recognit.*, vol. 37, no. 11, pp. 2245–2255, 2004.
- [32] M. Jaderberg, K. Simonyan, A. Zisserman et al., "Spatial transformer networks," *Proc. Adv. Neural Inf. Process. Syst.*, vol. 28, 2015.
- [33] B. Prommegger, C. Wimmer, and A. Uhl, "Rotation detection in finger vein biometrics using cnns," in *Proc. Int. Conf. Pattern Recognit.* IEEE, 2021, pp. 6531–6537.
- [34] B. Prommegger, C. Kauba, and A. Uhl, "On the extent of longitudinal finger rotation in publicly available finger vein data sets," in *Proc. Int. Conf. Biom., ICB*. IEEE, 2019, pp. 1–8.
- [35] J. Qiu, C. Chen, S. Liu, H.-Y. Zhang, and B. Zeng, "Slimconv: Reducing channel redundancy in convolutional neural networks by features recombining," *IEEE Trans. Image Process.*, vol. 30, pp. 6434–6445, 2021.
- [36] Y. Yin, L. Liu, and X. Sun, "Sdumla-hmt: A multimodal biometric database," in *Proc. Lect. Notes Comput. Sci.* Springer, 2011, pp. 260–268.

- [37] B. T. Ton and R. N. Veldhuis, "A high quality finger vascular pattern dataset collected using a custom designed capturing device," in *Proc. Int. Conf. Biom., ICB*. IEEE, 2013, pp. 1–5.
- [38] M. S. M. Asaari, S. A. Suandi, and B. A. Rosdi, "Fusion of band limited phase only correlation and width centroid contour distance for finger based biometrics," *Exp. Syst. Appl.*, vol. 41, no. 7, pp. 3367–3382, 2014.
- [39] A. Kumar and Y. Zhou, "Human identification using finger images," *IEEE Trans. Image Process.*, vol. 21, no. 4, pp. 2228–2244, 2011.
- [40] F. Svanström, C. Englund, and F. Alonso-Fernandez, "Real-time drone detection and tracking with visible, thermal and acoustic sensors," in *Proc. Int. Conf. on Pattern Recog.* IEEE, 2021, pp. 7265–7272.
- [41] M. Gomez-Barrero, J. Galbally, C. Rathgeb, and C. Busch, "General framework to evaluate unlinkability in biometric template protection systems," *IEEE Trans. Inf. Forensics Security*, vol. 13, no. 6, pp. 1406–1420, 2017.
- [42] M. Gomez-Barrero and J. Galbally, "Reversing the irreversible: A survey on inverse biometrics," *Comput. Secur.*, vol. 90, p. 101700, 2020.
- [43] D. Sathya and B. Raman, "Generation of cancelable iris templates via randomized bit sampling," *IEEE Trans. Inf. Forensics Security*, vol. 14, no. 11, pp. 2972–2986, 2019.
- [44] D. P. Kingma and J. Ba, "Adam: A method for stochastic optimization," *arXiv preprint arXiv:1412.6980*, 2014.
- [45] R. R. Selvaraju, M. Cogswell, A. Das, R. Vedantam, D. Parikh, and D. Batra, "Grad-cam: Visual explanations from deep networks via gradient-based localization," in *Proc. IEEE Conf. Comput. Vis. Pattern Recog.*, 2017, pp. 618–626.
- [46] R. Das, E. Piciuccio, E. Maiorana, and P. Campisi, "Convolutional neural network for finger-vein-based biometric identification," *IEEE Trans. Inf. Forensics Security*, vol. 14, no. 2, pp. 360–373, 2018.
- [47] S. Prasad and T. Chai, "Multi-scale arc-fusion based feature embedding for small-scale biometrics," *Neural Processing Letters*, pp. 1–18, 2023.
- [48] L. Zhang, L. Sun, W. Li, J. Zhang, W. Cai, C. Cheng, and X. Ning, "A joint bayesian framework based on partial least squares discriminant analysis for finger vein recognition," *IEEE Sens. J.*, vol. 22, no. 1, pp. 785–794, 2021.
- [49] P. Zhao, S. Zhao, J.-H. Xue, W. Yang, and Q. Liao, "The neglected background cues can facilitate finger vein recognition," *Pattern Recog.*, vol. 136, p. 109199, 2023.
- [50] N. Aherrahrou and H. Tairi, "A novel cancelable finger vein templates based on ldm and retinexgan," *Pattern Recog.*, vol. 142, p. 109643, 2023.
- [51] X. Zhang, H. Wang, L. Ye, and L. Tao, "Finger-vein cancelable template protection based on random permutation projection," in *Proc. Int. Conf. Signal Image Process., ICSIP*. IEEE, 2020, pp. 709–713.
- [52] S. K. Choudhary and A. K. Naik, "Multi-instance finger vein-based authentication with secured templates," *Int. J. Adv. Comput. Sci. Appl.*, vol. 13, no. 5, 2022.
- [53] X. Hu, L. Zhang, H. Wang, J. Zhou, and L. Tao, "Dual hashing index cancellable finger vein template based on gaussian random mapping," *Symmetry*, vol. 14, no. 2, p. 258, 2022.